ECCM-17TH EUROPEAN CONFERENCE ON COMPOSITE MATERIALS
Munich, Germany, 26-30 June 2016

MULTISCALE MODELLING AND SIMULATION OF FAILURE IN METAL-COMPOSITE INTERFACES

F. Hirsch *[1], M. Kästner[1]

[1] *Institute of Solid Mechanic, Chair of Nonlinear Solid Mechanics, Technische Universität Dresden,George-Bähr-Str. 3c, 01062 Dresden*
* *Corresponding Author: franz.hirsch@tu-dresden.de*

Keywords: interface, roughness, cohesive, multiscale

Abstract
In this contribution the inelastic behavior of bi-material interfaces is considered. We study different local phenomena and their effects on the overall interface characteristics, e.g. the elastic mismatch of the bi-material interface and the surface roughness. Since there is a large separation in the length scales of the surface roughness, which is in the micrometer range, and conventional structural components, we employ a numerical homogenization approach to extract effective interface parameters. The description of interface failure is based on cohesive elements in combination with a traction-separation law.

1. Introduction

The application of fiber reinforced plastics (FRP) in multi-material lightweight structures requires innovative joining concepts to combine the advantages of FRP with conventionally lightweight materials as aluminum. Such hybrids are essential to realize appropriate load transfer elements in automotive or aircraft industry. Different from technologies like bolted or riveted joints, which generally induce damage in the composite material, approaches that create the connection during the forming process itself instead of a subsequent joining step are promising solutions. Despite the intrinsic joining process, the failure of the structure is often initialize in the bonding zone as shown in Fig. 1. One possibility to optimize the adhesion of the bi-material interface is the design of structured surfaces to improve the mechanical interlock. As shown in Fig. 1 the roughness of the interface could be increased with a sandblast pre-treatment of the aluminum surface.
In the following we consider the interface failure behavior on the microscale and the influence of a certain interface roughness. Since there is a large separation of length scales, numerical multiscale simulation techniques are a suitable means to investigate the local phenomena in the vicinity of the interface and to predict effective interface properties.
The description of the local material structure is based on the finite element method in combination with cohesive elements. This allows for the consideration of discontinuities within the material due to interface failure.

Excerpt from ISBN 978-3-00-053387-7

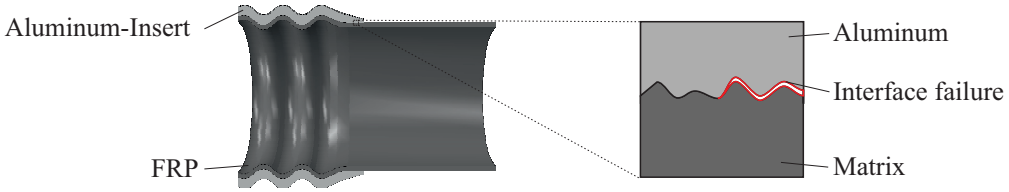

Figure 1. Intrinsic hybrid consisting of aluminum insert and fiber reinforced plastic (FRP) and failure of the bi-material interface of aluminum and matrix material.

2. Constitutive models

Since only adhesive failure as dissipative mechanism is considered here, the bulk behavior is modelled as isothermal linear elastic material

$$\boldsymbol{\sigma}^{\mathrm{m}} = 2\mu\boldsymbol{\varepsilon}^{\mathrm{m}} + \lambda\mathrm{trace}(\boldsymbol{\varepsilon}^{\mathrm{m}})\mathbf{I} \tag{1}$$

with the Lamé parameters $\mu = E/(2(1+\nu))$ and $\lambda = E/((1+\nu)(1-2\nu))$ depending on the Youngs's modulus E and the *Poisson*'s ratio ν. The inelastic behavior of the interface is described in terms of a cohesive zone model. Therefor the process zone ahead the crack tip is determined by a bilinear traction-separation law (TSL) proposed by Camanho et al. [1]

$$\mathbf{t}_{\mathrm{c}} = (1-D)\left(k_{\mathrm{n}}\langle[[u_{\mathrm{n}}]]\rangle_{+}\mathbf{n} + k_{\mathrm{s}}[[u_{\mathrm{s}}]]\mathbf{s}\right) + k_{\mathrm{n}}\langle[[u_{\mathrm{n}}]]\rangle_{-}\mathbf{n} \tag{2}$$

with the elastic stiffness k_I and separations $[[u_I]]$ in normal $I = \mathrm{n}$ and shear direction $I = \mathrm{s}$, respectively. The normal and shear unit vectors $\mathbf{n}$ and $\mathbf{s}$ correspond to the local interface orientation. The Macaulay brackets ensure that the damage variable D only affects the normal stiffness under tension loading to prevent interface penetration under compression loading. The schematic representation of the TSL is shown in Fig. 2 (a). After a linear slope, damage is initialized triggered by the quadratic stress criterion

$$\left(\frac{\langle t_{\mathrm{n}}\rangle}{t_{\mathrm{n}}^{0}}\right)^{2} + \left(\frac{t_{\mathrm{s}}}{t_{\mathrm{s}}^{0}}\right)^{2} - 1 = 0 \tag{3}$$

with the traction coordinates t_I and the cohesive strengths t_I^0. Afterwards, a linear decrease of the elastic stiffness k_I follows which is driven by a power law criterion

$$\left(\frac{G_{\mathrm{I}}}{G_{\mathrm{cI}}}\right)^{a} + \left(\frac{G_{\mathrm{II}}}{G_{\mathrm{cII}}}\right)^{a} - 1 = 0 \tag{4}$$

with the pure mode energy release rates G_I, the critical energy release rates $G_{\mathrm{c}I}$, $I = \mathrm{I,II}$ and the exponent a to weight the mixed mode behavior.

3. Homogenization

The homogenization scheme used for the finite element simulations in Section 4 was proposed by Alfaro et al. [2] and already adopted in e.g. [3] and [4]. Based on the Hill-Mandel energy condition, an appropriate criterion for interface considerations can be formulated

$$\mathbf{t}_{\mathrm{c}}^{\mathrm{M}} \cdot \delta[[\mathbf{u}^{\mathrm{M}}]] = \frac{1}{b}\int_{\Gamma^{\mathrm{m}}} \mathbf{t}^{\mathrm{m}} \cdot \delta\mathbf{u}^{\mathrm{m}}\mathrm{d}\Gamma \tag{5}$$

Excerpt from ISBN 978-3-00-053387-7

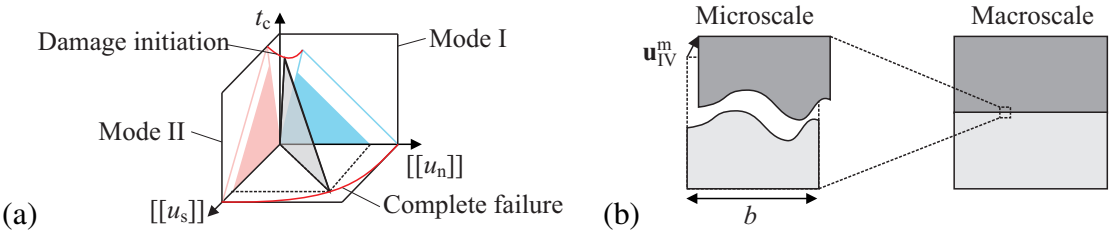

Figure 2. Schematic representation of (a) the bilinear traction-separation law used for cohesive zone elements and (b) the approach for interface homogenization.

where the virtual work on the macroscale (indicated with $(\cdot)^M$) done by the cohesive traction $\mathbf{t}_c^M$ and the separation $[[\mathbf{u}^M]]$ equals the volume average of the work done on the microscale (indicated with $(\cdot)^m$) by the boundary tractions $\mathbf{t}^m$ and displacements $\mathbf{u}^m$. The width b of the micro domain is used for the averaging step. With the formulation of the macroscopic separation in terms of the displacement of one control node of the micro domain $[[\mathbf{u}^M]] = \mathbf{u}^m_{IV}$ (see Fig. 2 (b)) and incorporation of hybrid boundary conditions, the expression of the macroscopic traction in terms of the microscale quantities is reached:

$$\mathbf{t}_c^M = \frac{1}{b}\int_{\Gamma^m} \mathbf{t}^m \mathrm{d}\Gamma \tag{6}$$

With (6) and the displacement $\mathbf{u}^{IV}$ it is possible to extract an effective TSL and to determine the most important effective cohesive parameters, i.e. the strength t_{max}^{eff} and the effective critical energy release rate G_c^{eff} for mode I and mode II, respectively.

4. Simulation

In this section the presented constitutive models are used in combination with the homogenization scheme to study the failure behavior of a bi-material interface with a certain surface roughness. The investigated micromodel is shown in Fig. 3 (c) where the roughness profile is idealized with a sinusoidal profile. For natural surfaces with a periodic or random height profile there exist numerous measures to describe the characteristics in vertical and horizontal direction as for instance the arithmetic average or the autocorrelation length [5]. For the sinusoidal idealization, the characteristic surface height is determined by the amplitude A and the spatial variation by the wave length λ. Hence, the characteristic roughness measure in this contribution is the ratio A/λ. In addition to the roughness ratio, the influence of the material properties is investigated. Useful measures to characterize the mismatch of the elastic constants of bi-material interfaces are the Dundurs parameters [6]

$$\alpha = \frac{\mu_1(1-\nu_2) - \nu_2(1-\nu_1)}{\mu_1(1-\nu_2) + \nu_2(1-\nu_1)} \quad \text{and} \tag{7}$$

$$\beta = \frac{1}{2}\frac{\mu_1(1-2\nu_2) - \nu_2(1-2\nu_1)}{\mu_1(1-\nu_2) + \nu_2(1-\nu_1)} \quad \text{with} \tag{8}$$

$$\mu_i = \frac{E_i}{2(1+\nu_i)}, \tag{9}$$

where α depends on the Youngs's moduli E_i and β shows an additional dependence of the Poission's ratios ν_i, $i = 1, 2$. For the following studies only a mismatch in the elastic moduli is

Excerpt from ISBN 978-3-00-053387-7

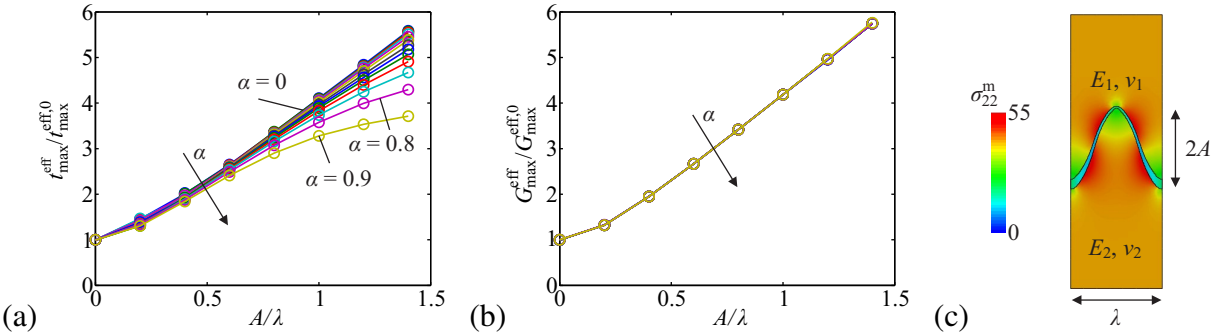

Figure 3. Simulation results of micromodel under tension conditions: (a) normalized effective strength $t^{\mathrm{eff}}_{\mathrm{max}}/t^{\mathrm{eff,0}}_{\mathrm{max}}$ and (b) normalized effective critical energy release rate $G^{\mathrm{eff}}_{\mathrm{max}}/G^{\mathrm{eff,0}}_{\mathrm{max}}$ depending on roughness ratio A/λ and (c) contour plot of micromodel with $\alpha = 0.4$ just after damage initiation.

investigated and the Poission's ratios were set equal $\nu_1 = \nu_2$. The results of the numerical simulations are shown in Fig. 3. The micromodel was loaded under tension conditions to simulate a macroscopic mode I failure of the interface. The cohesive zone model was parametrized to show isotropic behavior in normal and shear direction with a power law exponent $a = 1$. The influence of the dimensionless roughness on the effective traction $t^{\mathrm{eff}}_{\mathrm{max}}$ and effective critical energy release rate $G^{\mathrm{eff}}_{\mathrm{max}}$ is shown in Fig. 3 (a) and (b). Thereby the effective cohesive parameters were normalized to the values representing a flat interface with $A/\lambda = 0$. The parameter α indicates the mismatch in the elastic modulus and ranges from $\alpha = 0$ for identical properties and converges to $\alpha = 1$ for a large mismatch in the elastic properties. With increasing roughness ratio both effective cohesive parameters increase indicating an improvement of the global interface adhesion. The increased properties can be attributed to the increased surface area. Furthermore, a mismatch only affects the effective interface strength for high roughness ratios leading to lower values compared to the case with similar moduli. The range $0.9 \leq \alpha < 1$ is typical for material combinations made from aluminum and composite plastics. A contour plot of the domain just after damage initiation is shown in Fig. 3 (c) for the case with a stiff material 1 and a soft material 2 ($\alpha = 0.4$). The debonding starts at the indentation of material 2 resulting in stress concentrations at the edge of the hills. If cohesive failure was investigated in addition to adhesive failure, then material 2 would fail in this area.

5. Conclusion

The presented method enables the modelling of interface failure and the extraction of effective traction-separation relations of bi-material interfaces. Case studies show the influence of individual roughness parameters of the bi-material interface and demonstrate the general capability of the modelling strategy. It will be applied to analyze FRP-metal hybrid interfaces with cohesive failure in the future.

Acknowledgments: The present project is supported by the German Research Foundation (DFG) within the Priority Program (SPP) 1712, KA3309/4-1. This support is gratefully acknowledged.

Excerpt from ISBN 978-3-00-053387-7

References

[1] P. P. Camanho, C. G. Davila, and M. F. de Moura. Numerical simulation of mixed-mode progressive delamination in composite materials. *Journal of Composite Materials*, 37(16):1415–1438, 2003.

[2] M.V. Cid Alfaro, A.S.J. Suiker, C.V. Verhoosel, and R. de Borst. Numerical homogenization of cracking processes in thin fibre-epoxy layers. *European Journal of Mechanics - A/Solids*, 29(2):119–131, 2010.

[3] M. Kästner, S. Müller, F. Hirsch, J.-S. Pap, I. Jansen, and V. Ulbricht. XFEM modeling of interface failure in adhesively bonded fiber-reinforced polymers. *Advanced Engineering Materials*, 18(3):417–426, 2016.

[4] V. Palmieri and L. De Lorenzis. Multiscale modeling of concrete and of the FRP-concrete interface. *Engineering Fracture Mechanics*, 131:150–175, 2014.

[5] Qizhou Yao and Jianmin Qu. Interfacial versus cohesive failure on polymer-metal interfaces in electronic packagingeffects of interface roughness. *Journal of Electronic Packaging*, 124(2):127–134, 2002.

[6] J Dundurs. Discussion:edge-bonded dissimilar orthogonal elastic wedges under normal and shear loading(bogy, d.b., 1968, asme j. appl. mech., 35, pp. 460–466). *Journal of Applied Mechanics*, 36(3):650–652, 1969.

Excerpt from ISBN 978-3-00-053387-7